Renewable Energy 153 (2020) 1053–1066

Contents lists available at ScienceDirect

Renewable Energy

journal homepage: www.elsevier.com/locate/renene

A novel hybrid and interactive solar system consists of Stirling engine /vacuum evaporator thermoelectric cooler for electricity generation and water distillation

Moh'd A. Al-Nimr , Wahib A. Al-Ammari *

Department of Mechanical & Industrial Engineering, College of Engineering, Qatar University, Qatar

ARTICLE INFO

Article history:
Received 25 September 2019
Received in revised form
3 February 2020
Accepted 19 February 2020
Available online 22 February 2020

Keywords:
Hybrid solar system
Interactive solar system
Stirling engine
Thermoelectric cooler
Vacuum evaporator
Electricity generation and water distillation

ABSTRACT

This paper introduces a novel hybrid and interactive solar system to generate electricity and produce desalinated water. The system consists of a Stirling engine driven by concentrated solar radiation and cooled by saline water. Also, the system consists of an evacuated evaporator chamber to evaporate the saline water and thermoelectric cooler, driven by Stirling engine, to condensate the distilled water. The novelty of the system is in its positive interactivity since each component and product enhances the performance and productivity of others. The rejected heat from both the cold side of Stirling engine and the hot side of the TEC modules is used to heat the saline water before entering the evaporator. Also, the cold side of the TEC modules is used to enhance the condensation and hence the desalination rate. The importance of the second enhancement technique relays in the fact that many applications do not suffer from the absence of hot evaporative heating sources but suffer from the absence of condensation cool surfaces. A steady-state mathematical model has been proposed and validated by being compared with published data. The results show that at an optimized design point (solar radiation of 700 W/m2, wind speed of 5 m/s, swept volume of 210 cm^3, dish diameter of 2.68 m, etc.), the overall efficiency of the system was 65.8% with a net output power of 506 W and desalinated water of 28 kg/day. Including the TEC system has enhanced the condensation rate from 2.93 kg/day to 34.14 kg/day and the efficiency from 22.84% to 54.87%. Also, the two preheating effects (rejected heat from Stirling engine and from TEC modules) enhance the desalination rate from 2.93 kg/day to 11.74 kg/day and efficiency from 22.84% to 34.53%. Combining both enhancement techniques increase the desalination rate from 2.93 kg/day to 40.96 kg/day and efficiency from 22.84% to 64.44%.

1. Introduction

Most of the rural areas around the world suffer from a shortage of potable water and electricity. The solution to this problem by the traditional electrical power generation and water desalination plants is not feasible. This unfeasibility is due to the very high cost of them. Also, the infrastructures of these regions are not ready to build massive power and water plants. In addition to that, these rural regions randomly distribute, so large distributing networks are needed. The solar energy systems are a promised solution for this issue, especially in the areas that have a high solar radiation intensity. Solar stills, solar PV panels, and solar Stirling engines are examples of solar systems that form a solution for water and electricity problems. Some of these systems are in a commercial phase (such as PV panels and solar collectors) while the other are in the development phase (solar stills and solar dish systems). The essential criteria that make solar systems applications commercially feasible depend on three terms: simplicity, productivity, and cost. The researches still in progress toward a simple system with high productivity and low cost. Recently, the hybrid solar systems that provide electricity and distilled water were studied to reduce the capital and operating costs and to increase the productivity. However, these systems are more complex than the non-hybrid systems. This paper introduces a novel hybrid and interactive solar system that provides electricity and desalinated water by the combination of three units: solar Stirling engine, thermoelectric cooler (condenser), and vacuum evaporator. Before the clarification

* Corresponding author.
E-mail addresses: malnimr@just.edu.jo (M.A. Al-Nimr), wahib.alammari@qu.edu.qa (W.A. Al-Ammari).

https://doi.org/10.1016/j.renene.2020.02.072
0960-1481/

Nomenclature

A_d	area of the solar dish concentrator [m^2]
A_{ev}	cross-sectional area of the vacuum evaporation chamber [m^2]
A_{hr}	cross-sectional area of the hot side of the Stirling engine [m^2]
A_{cr}	cross-sectional area of the cold side of the Stirling engine. [m^2]
$A_{H,tec}$	surface area of the hot side of the TECMs [m^2]
$A_{C,tec}$	surface area of the cold side of the TECMs [m^2]
A_{sc}	surface area of the cooling coil over the cold side of the Stirling engine [m^2]
$a_f, a_{C,tec}$	constants were used on the Rayleigh numbers of the Stirling engine working fluid and of the evaporated vapor, respectively
B_n	Beal number of the Stirling engine
C	concentration ratio of the solar dish concentrator
C_s	solute concentration [%]
$c_{pw,2}$	Specific heat of the water inside the cooling coil of the Stirling engine [J/kg-K]
D_{cc}	diameter of the cooling coil of the Stirling engine [m]
D_d	diameter of the solar dish concentrator [m]
D_{hr}	diameter of the hot side of the Stirling engine (receiver) [m]
F	frequency of the Stilling engine cycle [Hz]
G	solar radiation intensity [$W/m^{2]}$
g	gravitational acceleration [m/s^2]
h_a	convective heat transfer coefficient from the solar dish receiver to the ambient air [W/m^2-K]
h_f	heat transfer coefficient of the free convection between the hot and cold chambers of the Stirling engine [W/m^2-K]
h_{cw}	heat transfer coefficient of the forced convection between the cooling coil surface and the cooling water of the Stirling engine [W/m^2-K]
$h_{H,tec}$	heat transfer coefficient of the forced convection between the hot side of the TECMs and the saline water [W/m^2-K]
$h_{C,tec}$	heat transfer coefficient of the free convection between the cold side of the TECMs and the saline water [W/m^2-K]
h_{fg}	latent heat of vaporization for water [J/kg]
I	electrical current of the TECMs [A]
k_f	thermal conductivity of the working fluid of the Stirling engine [W/m-K]
$k_{w,2}$	thermal conductivity of the saline water inside the cooling coil of the Stirling engine [W/m-K]
$k_{w,co}$	thermal conductivity of the evaporated water inside the condenser chamber [W/m-K]
$k_{H,tec}$	thermal conductivity of the water passes over the hot side of the TECMs [W/m-K]
L_f	spacing between the hot and cold plates of the Stirling engine [m]
L_{cc}	length of the cooling coil of the Stirling engine [m]
$L_{H,tec}$	length of the hot side of the TECMs [m]
$L_{C,tec}$	length of the cold side of the TECMs [m]
$\dot{m}_w$	mass flow rate of the saline water [kg/s]
$\dot{m}_{ev}$	mass flow rate of the evaporated water [kg/s]
$m_{distilled}$	mass of the condensed fresh water [kg/day]
Nu_f	Nusselt number of the free convection between the hot and cold chambers of the Stirling engine
$Nu_{w,2}$	Nusselt number of the forced convection between the cooling coil surface and the cooling water of the Stirling engine
$Nu_{H,tec}$	Nusselt number of the forced convection between the hot side of the TECMs and the saline water
$Nu_{C,tec}$	Nusselt number of the free convection between the hot side of the TECMs and the saline water
n_f, n_{tec}	constants were used on the Rayleigh numbers of the Stirling engine fluid and of the evaporated vapor, respectively
P_{SE}	generated power by the Stirling engine [W]
P_{VP}	power consumed by the vacuum pump [W]
P_{tec}	power consumed by the TECMs [W]
P_{net}	net electrical power generated by the system [W]
$Pr_{w,2}$	Prandtl number of the forced convection between the cooling coil surface and the cooling water of the Stirling engine
$Pr_{H,tec}$	Prandtl number of the forced convection between the hot side of the TECMs and the saline water
p_m	mean pressure inside the Stirling engine [Pa]
p_{atm}	atmospheric pressure [Pa]
p_{ev}	pressure inside the vacuum evaporator [Pa]
Q_{sun}	rate of heat supplied by the solar radiation on the solar dish [W]
Q_{dr}	rate of heat concentrated by the solar dish on the hot side of the Stirling engine [W]
$Q_{hr,a}$	rate of convective heat transfer from the hot side of the Stirling engine to the ambient air [W]
$Q_{hr,s}$	rate of radiative heat transfer from the hot side of the Stirling engine to the ambient air [W]
Q_{hc}	rate of convective heat transfer from the hot side of the Stirling engine to the cold side [W]
Q_{cw}	rate of convective heat transfer from the cold side of the Stirling engine to the saline cooling water [W]
$Q_{C,tec}$	rate of f convective heat transfer from the evaporated water to the cold side of the TECMs [W]
$Q_{H,tec}$	rate of convective heat transfer from the hot side of the TECMs to the saline water [W]
Q_{ev}	rate of heat absorbed from the condensed fresh water [W]
R_f	gas constant of the working fluid of the Stirling engine
Ra_f	Rayleigh number of the free convection between the hot and cold chambers of the Stirling engine
$Re_{w,2}$	Rayleigh number of the forced convection between the cooling coil surface and the cooling water of the Stirling engine
$Ra_{C,tec}$	Rayleigh number of the free convection between the hot side of the TECMs and the saline water
$Re_{H,tec}$	Rayleigh number of the forced convection between the hot side of the TECMs and the saline water
T_{hr}	temperature of the hot side chamber of the Stirling engine [K]
T_∞	air ambient temperature [K]
T_{sky}	temperature of the sky [K]
T_f	temperature of the working fluid of the Stirling engine [K]
T_{cr}	temperature of the cold side chamber of the Stirling engine [K]
$T_{m,2}$	mean temperature of the saline cooling water passes over the cold side of the Stirling engine [K]
$T_{2,o}$	outlet temperature of the saline cooling water passes over the cold side of the Stirling engine [K]

$T_{2,i}$	inlet temperature of the saline cooling water passes over the cold side of the Stirling engine [K]
$T_{m,3}$	mean temperature of the saline water passes over the hot side of the TECMs [K]
$T_{4,i}$	temperature of the saline water at the inlet of the vacuum evaporator [K]
T_{co}	temperature of the evaporated water inside the condenser [K]
$T_{C,tec}$	temperature of the cold side of the TECMs [K]
$T_{H,tec}$	temperature of the hot side of the TECMs [K]
V_{∞}	wind speed [m/s]
V_{SE}	swept volume of the Stirling engine [m^3]
$\dot{V}$	volume flow rate of the vacuum pump [m^3/s]
ρ_d	reflectivity of the solar dish concentrator
ρ_f	density of the working fluid of the Solar dish [kg/m^3]
$\rho_{w,2}$	density of the saline cooling water passes in the cooling coil of the Stirling engine [kg/m^3]
ε_{hr}	emissivity of the hot side of the Stirling engine
β_f	thermal expansion coefficient of the working fluid of the Stirling engine [1/K]
β_{co}	thermal expansion coefficient of the evaporated water inside the condenser [1/K]
σ	Stefan-Boltzmann constant [W/m^2-K^4]
$\mu_{w,2}$	dynamic viscosity of the saline cooling water passes in the cooling coil of the Stirling engine. kg/m-s
$\mu_{H,\ tec}$	dynamic viscosity of the saline water passes over the hot side of the TECMs [kg/m-s]
$\nu_{w,co}$	kinematic viscosity of the water vapor inside the condenser [m^2/s]
ν_f	kinematic viscosity of the working gas of the Stirling engine [m^2/s]
α_f	thermal diffusivity of the working fluid of the Stirling engine [m^2/s]
$\alpha_{w,co}$	thermal diffusivity of the water vapor inside the condenser [m^2/s]
α_m	mass modified accommodation factor
η_{SE}	efficiency of the Stirling engine
η_{system}	overall efficiency of the system

Abbreviations

SE	Stirling engine
HCSE	hot chamber of the Stirling engine
CCSE	cold chamber of the Stirling engine
TECMs	thermoelectric cooler modules

of the research gap of this work with its features and limitations, it is necessary to introduce a brief review of the current innovations, applications, and researches about these three units.

Solar dish concentrators are used in various applications such as electricity generation [1,2] steam generation [3], cooking [4],water desalination [5], heating air [6], refrigeration [7],and cogeneration of fresh water and electricity [8,9]. The electricity generation via the solar dish concentrators achieved by using the Rankine cycle [10], Brayton cycle [11,12], alkali metal thermal to electrical converter [13], or Stirling engine [14]. However, these systems still in research and investigation phase to enhance their efficiencies and solve the technical difficulties associated with their working conditions. A review about the evolution of dish design for a large number of concentrating solar power dish examples presented by Coventry et al. [15]. Wu et al. [13] proposed a system consists of a parabolic dish solar collector cascaded with an alkali metal thermal to electric converter (AMTEC) through a coupling heat exchanger. They reported that an overall conversion efficiency of the system could reach up to 20.6% with a power output of 18.54 kW at an operating temperature of 1280 K. Number of theoretical and experimental researches that studied the electricity generation by solar-powered Stirling engine are introduced. An experimental analysis and numerical validation of a solar Dish/Stirling system connected to the electric grid presented by Mendoza et al. [16]. They reported that for specified conditions, the Dish/Stirling system generates an electric power of 1.00 kW at a solar irradiation of 725 W/m^2 with a system overall efficiency of 17.6%. This experimental work was a validation for their published theoretical mathematical model of the same system [17]. Hafez et al. [18] introduce a modeling and simulation study for different parabolic dish Stirling engine designs using MATLAB program. They reported that at Zewail city of Science and Technology, Egypt, for a 10 kW Stirling engine, the maximum solar dish Stirling engine output power estimation is 9707 W at 12:00 p.m. where the maximum beam solar radiation applied in solar dish concentrator is 990 W/m^2.

Also, few papers studied the distillation of saline water using a solar still powered by a solar dish concentrator. Ameer et al. [19] discussed the potential of utilizing the rejected heat from a solar Stirling engine for water distillation. They have simulated the performance of the system using a mathematical model and real weather data. They mentioned that with a concentrator diameter of 10.57 m, the average water daily production is 22.5 kg of water. Prado et al. [20] introduced a dynamic simulation by computer for a solar dish used for desalting water and validated their simulation experimentally. They mentioned that the highest yield of distilled water was 4.95 kg/(m^2-day) with a galvanized steel parabolic dish of 0.68 m in height and 0.62 m in width. A design, manufacturing, and mathematical modeling of a parabolic dish concentrator with a novel solar still mounted at its focal point for saltwater desalination presented by Bahrami et al. [21]. They reported that for a dish concentrator with an aperture diameter of 3 m and specified conditions about 75 kg distilled water produced in a day for system operating from 8:30 a.mto 5:30 p.m. It can be noted that these proposed systems in Refs. [19,20], and [21] integrate the solar Stirling engine with distillation process with the absence of effective condensation. This yields a low productivity or requires higher dish diameter.

Recently, thermoelectric technology has incorporated within the solar systems. The thermoelectric systems are used in two different modes. The first mode is to generate electricity by absorbing heat from a high-temperature source and reject the residual heat to a cold sink utilizing thermoelectric generator modules (TEGMs). The second mode is to work as a refrigerator (or condenser) by transforming heat from a low-temperature source to a high-temperature sink utilizing thermoelectric cooler modules (TECMs) with consuming electrical power. In this work, we use the second mode. Many reviews about the use of TEG within the solar system applications were presented, such as [22,23]. Other reviews about the use of TEC in various applications were also presented, such as [24]. For example, the elevation of the PV cell's temperature reduces their efficiency and life time [25]. So, the TECMs can be used to cool them. This application was theoretically and experimentally studied in by Dimri et al. [26]. They studied two cases: case (a) PV partially covered with TEC, case (b) PV covered with TEC. They reported that the overall electrical efficiency of case (b) is higher than of case (b) by 4.46–6.23%. Another application of TECMs is to be used in a traditional solar still to elevate the temperature difference between the basin and the condensing sides.

This application theoretically explored by Dehghan et al. [27] and experimentally by Rahbar et al. [28]. The later reported that although the surface of TEC is approximately 2.8 times smaller than that of the glass, its productivity is 3.2 times higher. However, the rejected heat from the hot side of the TECMs of the presented systems (that use the TECMs in either to cool the PV modules [26] or to enhance the productivity of the solar stills [27,28]) is lost as waste heat. This waste heat could be recovered for further utilization as proposed in the present work. A few researches studied the integration of the TECMs with PV modules or with solar stills with the recovery of the rejected heat from them for further purposes. A theoretical study of a novel hybrid photovoltaic/thermoelectric cooler (PV/TEC) distillation system introduced by Al-Nimr et al. [29]. This work proposed to use the rejected heat from the TECMs for further water desalination. They mentioned that the maximum productivity of the system was at an ambient temperature of 298 K, solar radiation of 1000 W/m^2, wind speed of 5.5 m/s. It was 4.2 kg/day of distilled water and a net electrical output power of 73 W with an overall efficiency of 57.9% and PV cell efficiency of 12.32%. However, this system depends on the passive natural evaporation for the distillation process which is less efficient than the effective distillation by the evacuation process. An experimental study about the effective use of thermal energy at both the hot and cold sides of the thermoelectric modules used in a water distillation system introduced by Al-Madhhachi et al. [30]. The results of their experiments showed that the average water production is 28.5 mL/h with a specific energy consumption of 0.00114 kW h/mL in an evaporation chamber filled with $10 \times 10 \times 30$ mm^3 of water. Jradi et al. presents an experimental and theoretical study of an integrated thermoelectric–photovoltaic system for air dehumidification and freshwater production [31]. They perform a case study on the feasibility of implementing a thermoelectric-photovoltaic system in Beirut climate to produce at least 10 L of water per day through the summer months.

The desalination of saline water can be performed via traditional desalination plants that use various techniques such as multistage flash, multi-effect distillation, reverse osmosis, vapor compression, and electro-dialysis [32]. These conventional plants powered by fossil fuel, and this increases the emissions of greenhouse gases [33]. Also, these plants have expensive and complex structures with relatively high maintenance costs. Alternatively, these plants can be powered using solar energy. Generally, there are two categories of the desalination systems powered by solar energy: (a) Direct desalination systems which include (solar still, solar chimney, and solar humidification-dehumidification units), (b) indirect desalination systems which include (membrane-based processes and non-membrane-based processes). For more details about these processes, an excellent review of the solar desalination units is presented by Sharon and Reddy [34]. Also, a valuable review of the natural vacuum distillation for seawater desalination is published by Rashid et al. [35].

The core of the solar non-membrane desalination processes is the increase of saline water temperature (by solar collectors) and the creation of a vacuum (naturally or by using a vacuum pump). Within a vacuum evaporator, the evaporation process can occur at feed water temperature between 40 and 70 °C, which is achievable by solar heaters [36]. Number of desalination systems using the vacuum techniques are presented. However, these systems suffer from the absence of the sustainable power to drive the vacuum pumps or require high elevation to create natural vacuum. And, some systems use vacuum pumps and renewable sources for electricity, but the condensation process is not active (the electrical source only used to operate the pumps). A transient mathematical model of a novel multi-stage evacuated solar desalination system by utilizing latent heat recovery is presented by Reddy et al. [37]. Their proposed system consists of a flat plate collector (to raise the water temperature), a vacuum pump, a multi-stage evaporator, and a condenser chamber. This chamber designed such that the condenser surface at the bottom of one stage acts as the evaporator surface for the above one. They reported that the maximum yield of 53.2 kg/m^2/day found in March at an operating pressure of 0.03 bar. A natural vacuum desalination system installed with evacuated tube collectors is experimentally studied by Abbaspour et al. [38]. They mentioned that the highest hourly and daily productions were 1.134 kg/m^2-hr and 8.065 kg/m^2 day, respectively. Myneni et al. [39] proposed a natural vacuum desalination system integrated with thermoelectric generation modules powered by low-grade waste heat sources. They mentioned that the objective of their work is to achieve a proof of concept through an experimental model and thermal analysis. Also, a numerical and experimental work on the performance of a natural vacuum desalination system using a low-grade heat source is presented by Ambarita [40]. He concluded that the performance of the natural vacuum desalination system is mainly affected by the maximum temperature in the evaporator and the minimum temperature in the condenser. A novel vacuum desalination system powered by the waste heat of a steam power plant is proposed by Venkatesan et al. [41]. Their work experimentally performed within an existing thermal power plant in Chennai, India. They reported that the amount of the produced fresh water by this plant is nearly 1/200 times of the supplied sea water for an available temperature gradient of 8.7 °C.

Based on the above literature survey, it is clear that the already proposed systems in the literature suffer from one or more of these deficiencies: 1) the absence of effective active cooling technique (TEC), 2) the absence of renewable power to drive the vacuum pumps needed to enhance the evaporation rate, 3)the absence of effective utilization of the rejected heat from the system components, and 4) the absence of positive interactivity between all system components. The present work proposes an integrated system that overcomes all the previous deficiencies. It presents a solar dish Stirling engine integrated with a thermoelectric-cooler modules (condenser) and a vacuum evaporator connected with a vacuum pump. This assembly has number of important features: (a) the saline water used recover the rejected heat from the Stirling engine which improves the overall performance of the system, (b) the waste heat from the hot side of the thermoelectric cooler modules (TECMs) also recovered by the saline water to raise its temperature which facilitates the evaporation process inside the vacuum evaporator and minimizes the required power supplied to the vacuum pump, and (c) the presence of the TECMs enhance the evaporation process and provides an active condensation, (d) the proposed system provides electricity and desalinated water, simultaneously, and (e) the system considered as an eco-friendly system. It is worth mentioning that one of the most novel aspects of the proposed system is in its positive interactivity since the main three components (solar Stirling engine, thermoelectric cooler (condenser) and evaporator) support each other. The cooling of the Stirling engine raises the Stirling engine efficiency and the saline water temperature. Then, the saline water recovers the rejected heat by the TECMs, which further increases its temperature. Higher water temperature reduces the consumed power by the vacuum pump and enables more electricity to be used by the TECMs which increases the cooling effect. A higher cooling effect will also reject more heat that raises the saline water temperature and so on. In other words, higher cooling combined with lower evacuation power and more distilled water. Also, it is up to the designer to decide if more electric or more distilled water is required. However, the main drawback of the system is its high initial cost.

In this paper, section 2 introduces a detailed description of the system components and its overall operating mechanism. Section 3

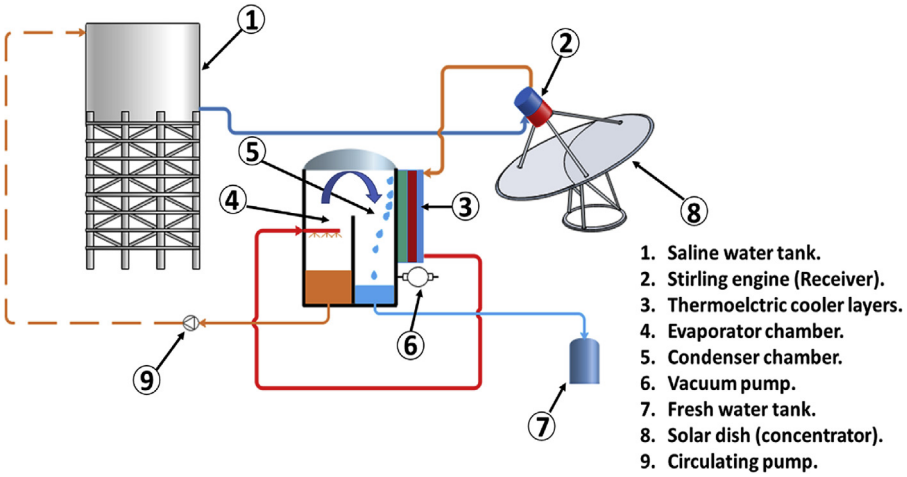

Fig. 1. Schematic diagram of the proposed system.

presents the steady-state mathematical model of the proposed system. Also, section 3 explained the solution method of the proposed model by using the Engineering Equation Solver (EES) program. Section 4 presents a model validation and a discussion about the effects of the main parameters on the performance of the system. Finally, section 5 summarizes the most important results obtained in the simulation process.

2. System description

The proposed system consists of the shown components in Fig. 1. The main components of the system are: the solar dish Stirling engine unit (2,8), the thermoelectric cooler (condenser) (3,5), the evaporator chamber (4), the vacuum pump (6), the circulating pump (9), the storage tank of the saline water (1), and the storage tank of the desalinated water (7).

Now, the overall mechanism of the system (shown in Fig. 1) is explained as: (a) the solar dish concentrates the solar radiation of the sun on the receiver (hot chamber of the Stirling engine), (b) the receiver converts the solar energy into thermal energy and raise the temperature of the engine working fluid, (c) the Stirling engine convert part of the absorbed energy into mechanical energy then into electrical energy, while the other part rejected to the cold chamber and to the ambient atmosphere, (d) the saline water flows over the cold chamber and recover the rejected heat by the engine, this raises the saline water temperature, (e) then, the saline water flows over and recover the rejected heat from the hot side of the TECMs which further increase the temperature of the saline water, (f) then, the saline water flows into the vacuum evaporator chamber which is kept at a pressure lower than the saturated pressure of the saline water (by a vacuum pump), (g) part of the saline feed water flashed into vapor while the remainder being recirculated to the storage tank by the circulating pump, (h) finally, the produced vapor transferred to the condenser chamber and condensed by losing heat to the cold side of the TECMs. The required power to operates the TECMs, Vacuum pump and circulating pump provided by the Stirling engine generator.

3. Mathematical modeling

The mathematical model of the system includes the formulations of three units: the solar dish Stirling engine, the TECMs, and the vacuum evaporator. To simplify the thermodynamic model; the following assumptions were made:

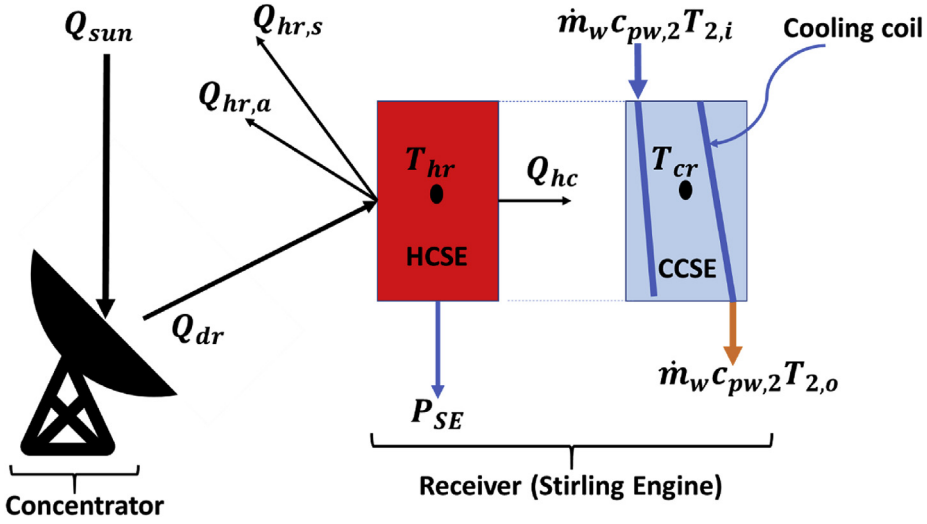

Fig. 2. Energy transfer processes in the Solar dish Stirling engine system.

- The system operates under steady-state conditions.
- The properties of all fluids are obtained at the average temperatures of their mediums.
- The temperature of the hot chamber of the Stirling engine equals the temperature of the receiver.
- The variations in the kinetic and potential energies are neglected.
- The internal friction of the fluid with the pipes is neglected.
- The temperature of the saline water at the exit of the cooling coil equals to that at the inlet of the TECMs unit ($T_{2,o} = T_{3,i}$).
- The temperature of the saline water at the exit of the TECMs unit equals to that at the inlet of the vacuum evaporator ($T_{3,o} = T_{4,i}$).

Starting with the modeling of the solar dish Stirling engine, the steady-state energy balance equation over the hot chamber of the Stirling engine (HCSE), as shown in Fig. 2, can be written as:

$$Q_{dr} - Q_{hr,a} - Q_{hr,s} - P_{SE} - Q_{hc} = 0 \tag{1}$$

where Q_{dr} is the concentrated solar energy by the solar dish on the receiver (hot chamber), $Q_{hr,a}$ is the heat losses by convection from the hot chamber (HCSE) to the ambient air, $Q_{hr,s}$ is the heat losses by radiation between the HCSE and the sky, P_{SE} is the power generated by the Stirling engine, and Q_{hc} is the heat rejected by the engine to the cold chamber. The concentrated energy by the solar dish on the receiver is given by Ref. [18]:

$$Q_{dr} = \rho_d A_{hr} C G \tag{2}$$

It can be noted that Q_{dr} depends on the solar radiation intensity G, reflectivity of the solar dish ρ_d, and the area of the concentrator A_d which is mathematically included within the concentration ratio of the solar dish C that given as [18]:

$$C = A_d / A_{hr} \tag{3}$$

where A_{hr} is the area of the receiver (HCSE). The area of the concentrator is given in terms of the solar dish diameter in Eqn. (4). The area of the HCSE is given in term of the receiver diameter in Eqn. (5) as [18].

$$A_{hr} = \pi \frac{D_{hr}^2}{4} \tag{4}$$

$$A_d = \pi \frac{D_d^2}{4} \tag{5}$$

Also, $Q_{hr,a}, Q_{hr,s}$ are given by Ref. [42]:

$$Q_{hr,a} = h_a A_{hr} (T_{hr} - T_\infty) \tag{6}$$

$$Q_{hr,s} = \varepsilon_{hr} \sigma A_{hr} \left(T_{hr}^4 - T_{sky}^4 \right) \tag{7}$$

here, h_a is the convection heat transfer coefficient between the HCSE and the ambient air, A_{hr} is the area of the receiver (HCSE), T_{hr} is the temperature of the HCSE, T_∞ is the temperature of the ambient air, ε_{hr} is the emissivity of the receiver, and T_{sky} is the effective temperature of the sky. h_a and T_{sky} are given by Refs. [43,44]:

$$h_a = 5 + 3.8 V_\infty \tag{8}$$

$$T_{sky} = 0.0552 \times T_\infty^{1.5} \tag{9}$$

The power generated by the Stirling engine P_{SE} is given by Ref. [45]:

$$P_{SE} = F V_{SE} p_m B_n \tag{10}$$

where F is the engine cycle frequency of the Stirling engine, V_{SE} is the swept volume of the Stirling engine, p_m is the mean pressure of the working fluid of the Stirling engine, and B_n is the Beale number. Here, P_m is given by Ref. [45]:

$$p_m = \rho_f R_f T_f \tag{11}$$

where ρ_f is the density of the working fluid of the Stirling engine (SE), R_f is the gas constant, T_f is the average temperature of the working fluid of the SE. T_f is given in terms of the hot chamber temperature T_{hr} and cold chamber temperature T_{cr} as [45]:

$$T_f = \frac{T_{hr} + T_{cr}}{2} \tag{12}$$

The rejected heat through the cold chamber of the Stirling engine (CCSE) to the cooling saline water is given as [42]:

$$Q_{hc} = h_f A_{hr} (T_{hr} - T_{cr}) \tag{13}$$

where h_f is the free convection heat transfer coefficient between the fluid in the hot and cold chambers which is given in terms of Rayleigh and Nusselt numbers as [46]:

$$Nu_f = h_f \times \frac{L_f}{k_f} \tag{14}$$

$$Nu_f = a_f \times Ra_f^{n_f} \tag{15}$$

$$Ra_f = \frac{g \beta_f (T_{hr} - T_{cr}) L_f^3}{\nu_f \alpha_f} \tag{16}$$

All parameters that presented in Eqn. (14–16) were explained in the nomenclature. Also, the rejected heat to the saline cooling water is given in terms of the forced convection between the cold chamber and the water as [42]:

$$Q_{hc} = h_{cw} A_{sc} (T_{cr} - T_{m,2}) \tag{17}$$

where $T_{m,2}$ is the mean temperature of the saline water through the cooling coil of the SE, A_{sp} is the surface area of the cooling coil, h_{cw} is the forced convection heat transfer coefficient between the CCSE and the cooling water which is given in term of Reynolds, Nusselt, and Prandtl numbers as [47]:

$$T_{m,2} = \frac{T_{2,i} + T_{2,o}}{2} \tag{18}$$

$$Nu_{w.2} = h_{cw} \times \frac{L_{cc}}{k_{w.2}} \tag{19}$$

$$Nu_{w,2} = 0.023 \times Re_{w,2}^{4/5} \times Pr_{w,2}^{0.4} \tag{20}$$

$$Re_{w,2} = \frac{4 \dot{m}_w}{\pi \mu_{w,2} D_{cc}} \tag{21}$$

$$A_{sc} = \pi D_{cc} L_{cc} \tag{22}$$

All parameters that mentioned in the Eqn. (18–20) were explained in the nomenclature. In terms of the mass flow rate of the

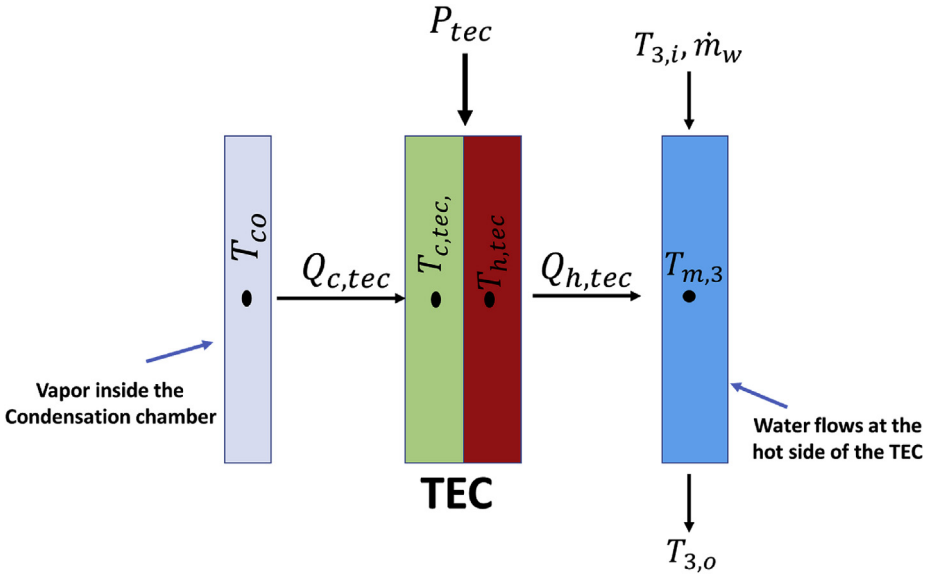

Fig. 3. The energy transfer processes in the thermoelectric cooling system.

saline water $\dot{m}_w$, the inlet temperature of the saline water into the cooling coil $T_{2,i}$, and the outlet temperature of the saline water from the cooling coil $T_{2,o}$, the rejected heat by the CCSE (recovered by the saline water) is given as:

$$Q_{cw} = \dot{m}_w c_{pw,2} (T_{2,o} - T_{2,i}) \quad (23)$$

Now, the model of the thermoelectric cooler modules will be presented. As shown in Fig. 3, the heat absorbed by the cold side of the TECMs from the condenser $Q_{C,tec}$ is given as [42]:

$$Q_{C,tec} = h_{C,tec} A_{C,tec} (T_{co} - T_{C,tec}) \quad (24)$$

where $A_{C,tec}$ is the surface area of the cold side of the TECMs, T_{co} is the temperature of the vapor inside the condenser, $T_{C,tec}$ is the temperature of the cold side of the TECMs, and $h_{C,tec}$ is the free convection heat transfer coefficient between the vapor and the cold

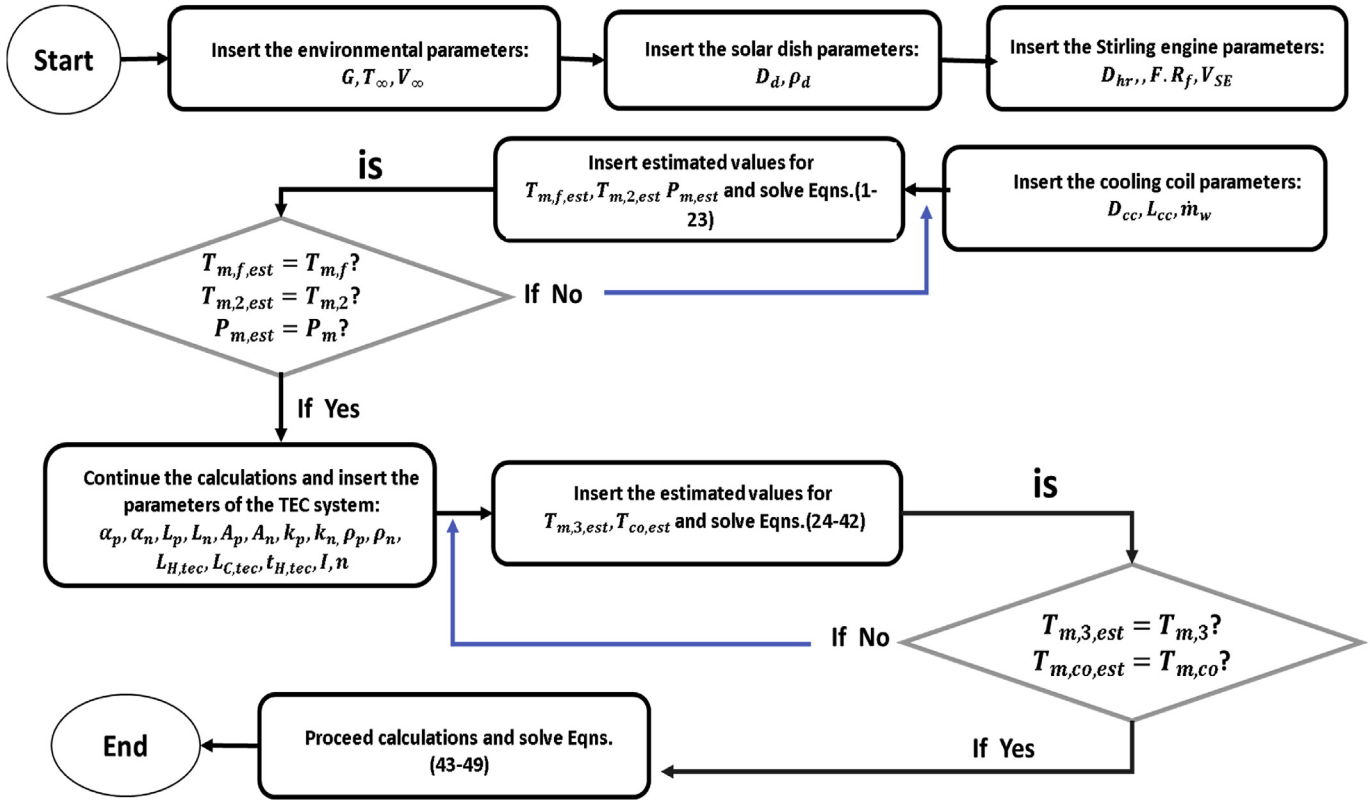

Fig. 4. Flow chart of the procedures followed to solve the model of the system.

Table 1
The input parameters of the proposed system.

Item	Value	unit
Environmental parameters		
Solar radiation intensity, G	300–1000	W/m^2
Wind speed, V_∞	0.5–12	m/s
Ambient temperature, T_∞	300–310	K
Solar dish concentrator and receiver parameters		
Solar dish diameter, D_d	2.68	m
Reflectivity of the solar dish material, ρ_d	0.98	
Diameter of the hot side of the receiver, D_{hr}	0.2	m
Emissivity of the receiver, ε_{hr}	1	
Stirling engine parameters		
Working fluid	Air	
Swept volume, V_{SE}	210	cm^3
Beale number, B_n	0.16	
Gas constant, R_f	287	J/kg-K
Engine cycle frequency, F	25	Hz
Cooling coil parameters		
Diameter of the cooling coil, D_{cc}	0.03	m
Length of the cooling coil, L_{cc}	2	m
Mass flow rate of the saline cooling coil, $\dot{m}_w$	0.02	kg/s
TECMs parameters		
Seebeck coefficient	$\alpha_p = \alpha_n = 3.47 \times 10^{-4}$	V/K
Thermal conductivity	$k_p = k_n = 0.97$	W/m-K
Electrical resistivity	$\rho_p = \rho_n = 1.33 \times 10^{-5}$	Ω.m
Length of the legs	$L_p = L_n = 1.4$	mm
Cross-sectional area of the legs	$A_p = A_n = 19$	mm^2
Number of thermoelectric leg pairs	$n = 12000$	
Vacuum evaporator parameters		
Vacuum pump efficiency, η_{VP}	0.85	
Mass modified accommodation factor, α_m	10^{-7}	
Solute concentration, C_s	3.5	%
Cross-sectional area of the evaporator, A_{ev}	0.2	m^2

side of the TECMs. $h_{C,tec}$ is given in terms of Rayleigh and Nusselt numbers as [46]:

$$Nu_{C,tec} = h_{C,tec} \times \frac{L_{C,tec}}{k_{w,co}} \tag{25}$$

$$Nu_{C,tec} = a_{c,tec} \times Ra_{C,tec}^{n_{c,tec}} \tag{26}$$

$$Ra_{C,tec} = \frac{g\beta_{co}(T_{co} - T_{C,tec})L_{C,tec}^3}{\nu_{w,co}\alpha_{w,co}} \tag{27}$$

And the heat rejected by the hot side of the TECMs to the saline water is given as [42]:

$$Q_{H,tec} = h_{H,tec}A_{H,tec}(T_{H,tec} - T_{m,3}) \tag{28}$$

where $A_{H,tec}$ is the surface area of the hot side of the TECMs, $T_{H,tec}$ is the temperature of the hot side of the TECMs, $T_{m,3}$ is the average temperature of the saline water through the TECMs unit (given in Eqn. (29)), and $h_{H,tec}$ is the forced convection heat transfer coefficient between the hot side of the TECMs and the saline water. $h_{H,tec}$ is given in terms of Reynolds, Nusselt, and Prandtl numbers as [47]:

$$T_{m,3} = \frac{T_{3,i} + T_{3,o}}{2} \tag{29}$$

$$Nu_{H,tec} = h_{H,tec} \times \frac{L_{H,tec}}{k_{w.3}} \tag{30}$$

Table 2
Comparison between the present system and Al-Dafaie et al. system.

Item	Al-Dafaie et al. [19]	Present Work
Main components of the system	Solar dish Stirling engine system cooled with a porous solar still installed on the cold side of the engine.	Solar dish Stirling engine system cooled with a saline water that distilled in a vacuum evaporator and condensed by TECMs condenser.
Type of the work	Theoretical	Theoretical
Main Parameters:		
Solar dish diameter	10.75 m	10.75 m
Receiver diameter	0.2 m	0.5 m
Reflectivity of the dish material	0.935	0.935
Solar radiation intensity	700	700
Net output power	14 kW	15.019 kW
Hot chamber temperature	1083 K	1231 K
Cold chamber temperature	330 K	330 K
Distillated water	24 kg/day	35 kg/day

Table 3
Comparison between the present system and Eames et al. system.

Item	Eames et al. [50]	Present Work
Main components of the system	Barometric desalination system powered by solar collector	Vacuum evaporator desalination system powered by solar dish Stirling engine and cooled by TECMs.
Type of the work	Experimental and theoretical	Theoretical
Compared Parameters:		
Solar collector/dish area	4.727 m^2	4.727 m^2
Feed-water mass flow rate	0.1 kg/s (average)	0.1 kg/s
Working pressure	0.5 kPa	17 kPa
Evaporator temperature Water	348 K (average)	309 K
productivity	30 kg/day	25 kg/day
Net electrical output power	No electrical power generated	950 W (average)
Best advantages	Lower cost Self-cooling system	Provides both electricity and desalinated water.
Major limitations	No electrical output Needs 10.3 m height to create a vacuum.	High initial cost.

$$Nu_{H,tec} = 0.023 \times Re_{w,3}^{4/5} \times Pr_{w.3}^{0.4} \tag{31}$$

$$Re_{H,\,tec} = \frac{4\dot{m}_w}{\pi \mu_{w.3} D_3} \tag{32}$$

In terms of the TECMs specifications, $Q_{C,tec}$, $Q_{H,tec}$ are given as [48]:

$$Q_{C,tec} = n \times \left[\alpha T_{C,tec} I - 0.5\, I^2 R + K\left(T_{C,tec} - T_{H,tec}\right)\right] \tag{33}$$

$$Q_{H,tec} = n \times \left[\alpha T_{H,tec} I + 0.5\, I^2 R + K\left(T_{C,tec} - T_{H,tec}\right)\right] \tag{34}$$

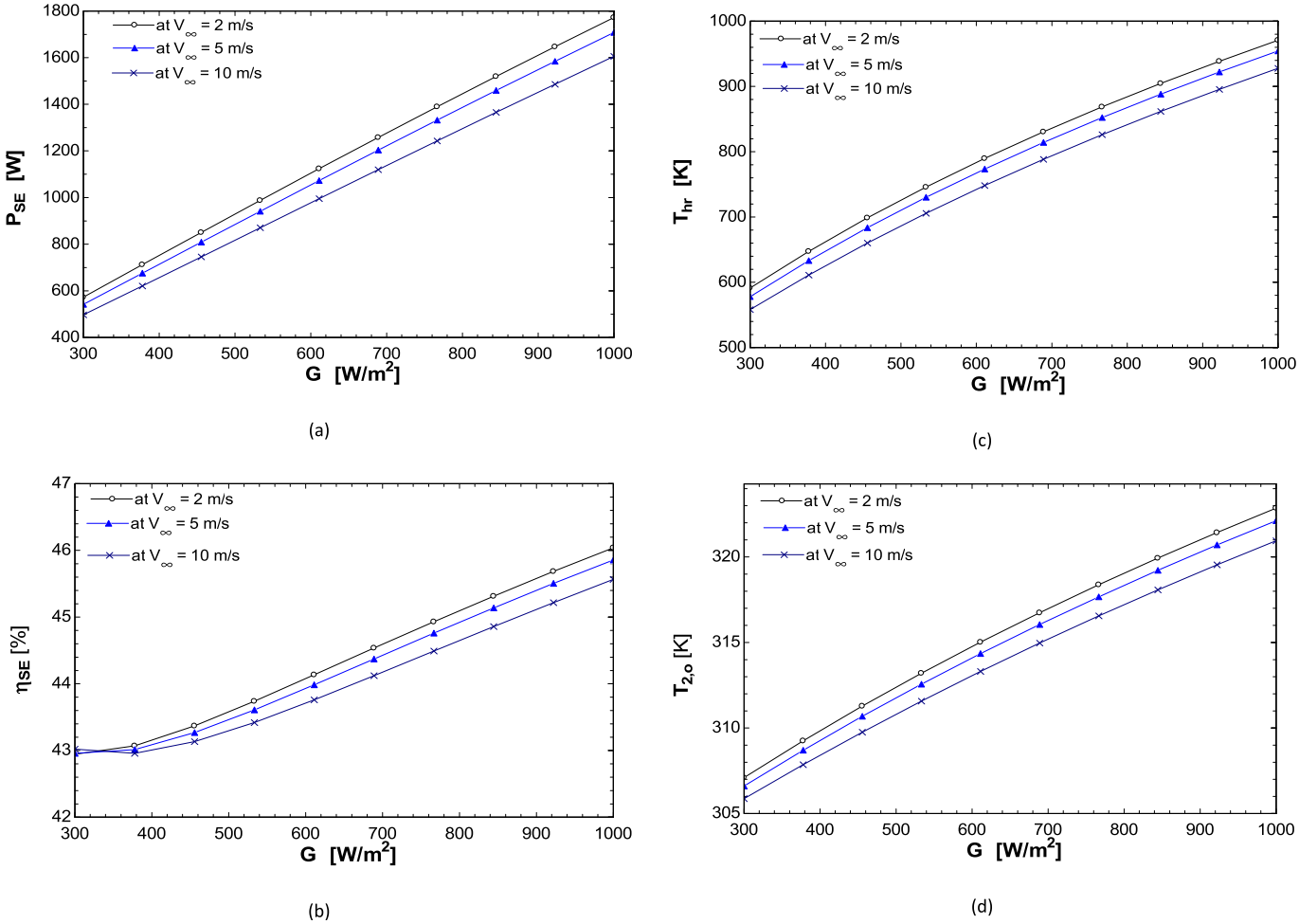

Fig. 5. Relationship between the solar radiation with the (a) output power of the Stirling engine, (b) efficiency of the Stirling engine, (c) engine hot chamber temperature, and (d) the outlet temperature of the saline cooling water at different wind speeds.

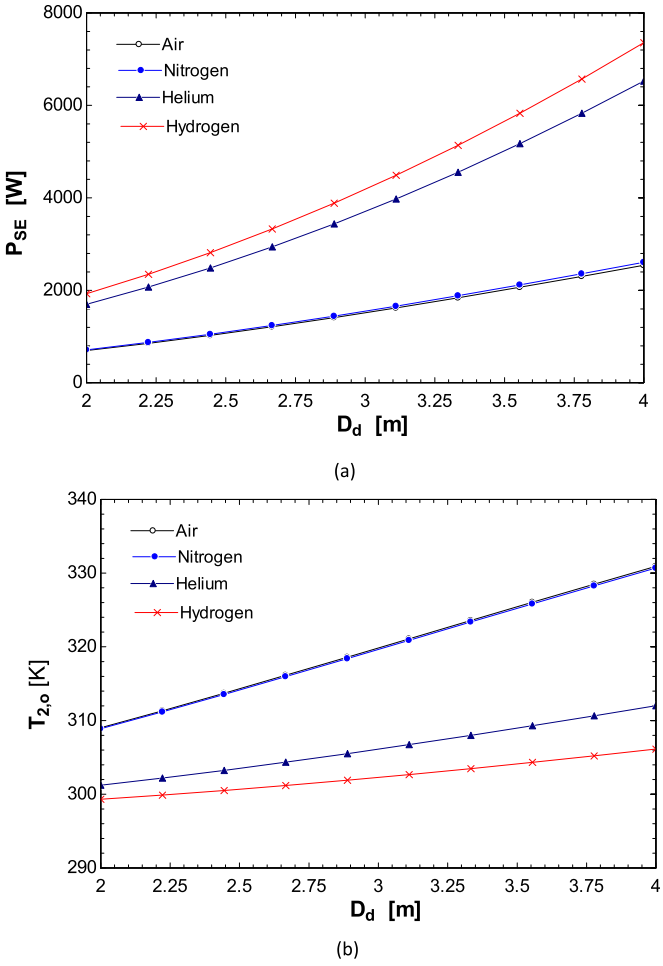

Fig. 6. The relationship between the solar dish diameter with the (a) output generated power and (b) outlet temperature of saline cooling water from the cold chamber of the SE for different working fluids.

$$\alpha = \alpha_p - \alpha_n \tag{35}$$

$$K = k_p \frac{A_p}{L_p} + k_n \frac{A_n}{L_n} \tag{36}$$

$$R = \rho_p \frac{L_p}{A_p} + \rho_n \frac{L_n}{A_n} \tag{37}$$

The power consumed by the TECMs is given as:

$$P_{tec} = Q_{H,tec} - Q_{C,tec} \tag{38}$$

Inside the vacuum evaporator, the evaporation rate is given as [35]:

$$\dot{m}_{ev} = \alpha_m A_{ev} \times \left[f(C_s) \frac{p(T_{4,i})}{\sqrt{T_{4,i}}} - \frac{p(T_{co})}{\sqrt{T_{co}}} \right] \tag{39}$$

$$f(C_s) = 1 - 0.0054\, C_s \tag{40}$$

where $p(T_{4,i})$ is the vapor pressure at the inlet temperature of the saline water into the vacuum evaporator and $p(T_{co})$ is the vapor pressure at the temperature of the condenser. The vapor pressure at a given temperature is given as [49]:

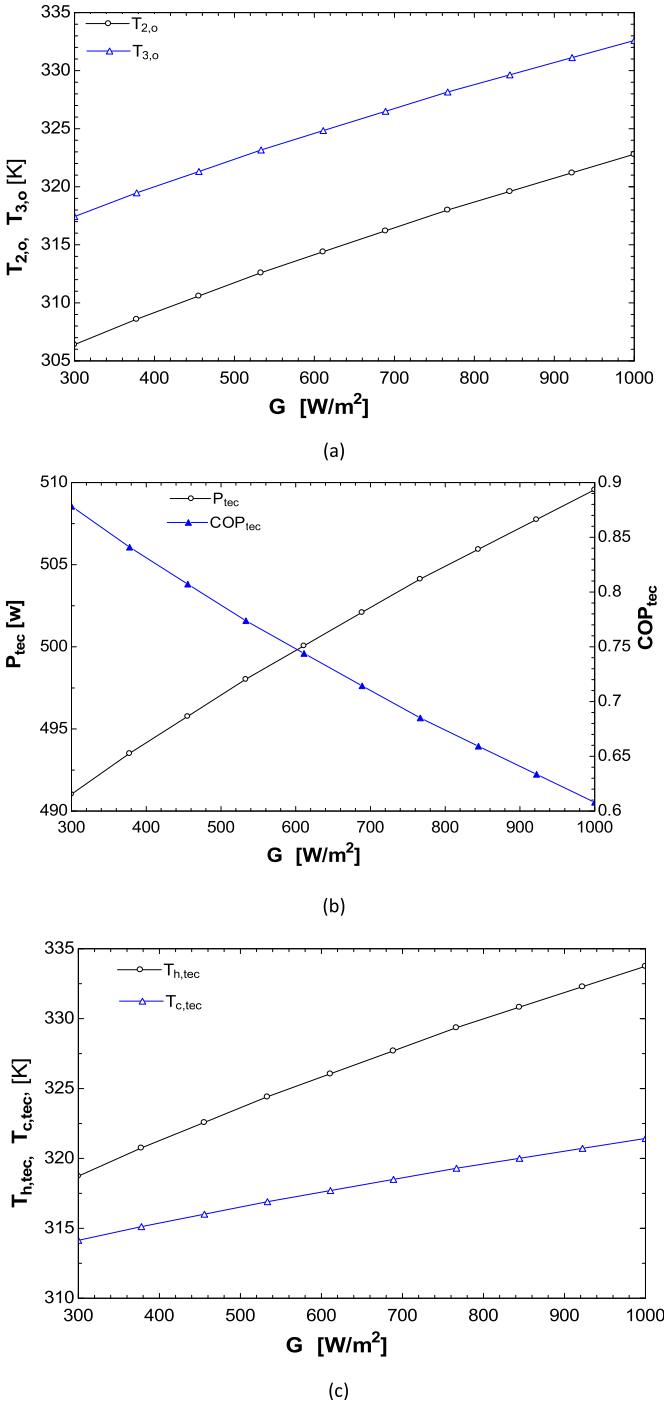

Fig. 7. The relationship between the solar radiation and the (a) temperatures of the saline water at the hot side of the TECMs, (b) the consumed power and the COP of the TECMs, and (c) the cold and hot side temperatures of the TECMs.

$$p(T) = 100 \times e^{\left(63.042 - \frac{713.6}{T} - 6.2558 \ln(T)\right)} \tag{41}$$

The power consumed by the vacuum pump is estimated as:

$$P_{VP} = \dot{V}(P_{atm} - P_{ev})/\eta_{VP} \tag{42}$$

$$\dot{V} = \dot{m}_{ev}/\rho_{w,ev} \tag{43}$$

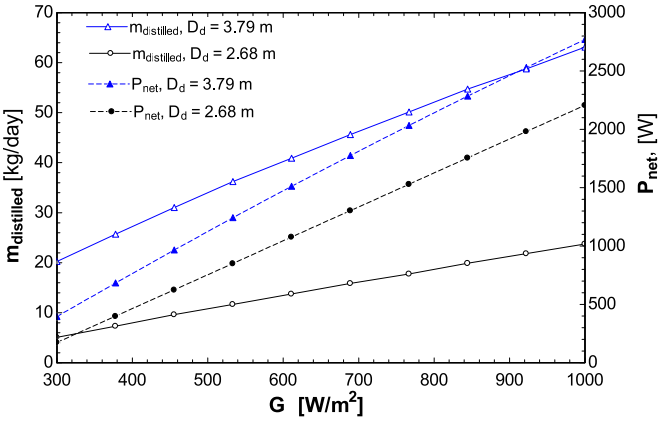

(a)

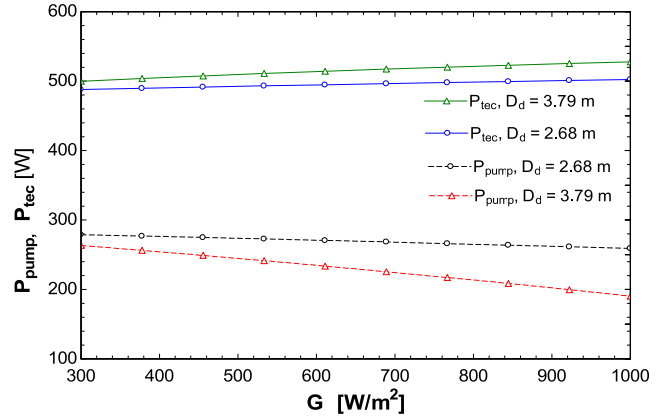

(b)

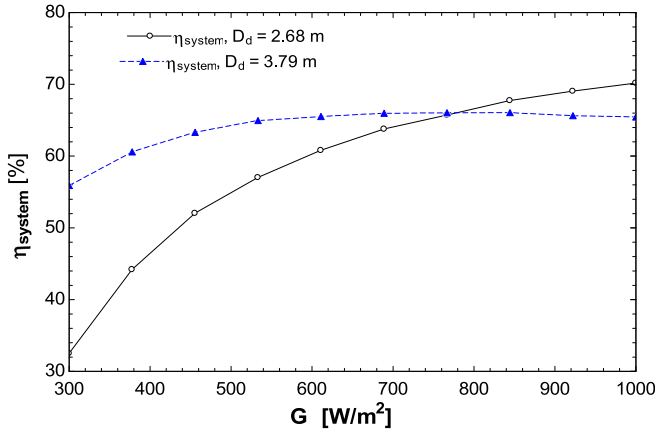

(c)

Fig. 8. The relationship between the solar radiation and the (a) daily productivity and net output power of the system, (b) consumed power by the TECMs and the vacuum pump, and (c) the overall efficiency of the system at different solar dish diameters.

Finally, to assist the performance of the system, the efficiency of the Stirling engine, the net electrical output, the daily desalinated water, and the overall efficiency of the system are given as:

$$\eta_{SE} = 100 \times \frac{P_{SE}}{(P_{SE} + Q_{hc})} \tag{44}$$

$$P_{net} = P_{SE} - (P_{tec} + P_{VP}) \tag{45}$$

$$m_{distilled} = \dot{m}_{ev} * 3600 * N_{hrs} \tag{46}$$

$$\eta_{system} = \frac{P_{net} + Q_{ev}}{Q_{sun}} \tag{47}$$

where Q_{ev} is the required heat to evaporate the saline water and given in Eqn. (48), Q_{sun} is the solar power incident on the solar dish concentrator and given in Eqn. (47).

$$Q_{ev} = \dot{m}_{ev} h_{fg} \tag{48}$$

$$Q_{sun} = G A_d \tag{49}$$

The previous equations (1–49) were solved simultaneously by using the Engineering equation solver (EES) with trial and error approach, as shown in the flow chart in Fig. 4. The input data through the simulation process are listed in Table 1. It should be mentioned that the environmental data were selected based on the nominal conditions of the summer season in Jordan.

4. Results and discussion

In this part of the paper, the validation of the proposed model is presented via the comparison with theoretical and experimental published works under the same conditions. Also, the effects of the major parameters on the performance of the system were discussed. This is done by changing the value of a parameter while the other parameters keep fixed at the values presented in Table 1.

4.1. Model validation

To validate the proposed thermodynamic model of the present system; the obtained results compared with published theoretical and experimental results of previous similar works. The results of the solar dish Stirling engine with the desalination process are compared with the theoretical published work by Al-Dafaie et al., as shown in Table 2. The fundamental difference between the systems is in the desalination method. Al-Dafaie et al. system uses a porous desalination unit installed on the cold chamber of the Stirling engine, while the present work uses a vacuum evaporator with TECMs condenser. For the same major parameters, the results show a good agreement (see Table 2). The diameter of the hot receiver in the present work selected to be 0.5 m at a solar dish diameter of 10.57 m. This is due that the use of 0.2 m receiver diameter results in a divergent solution. Also, since the present system uses an effective evaporation and condensation methods, the productivity is higher.

Table 3 shows a comparison between the present work and the theoretical and experimental published work by Eames et al. [50]. The major differences between the compared systems are in the method of receiving solar energy, the cooling method, and the output of the system. The present work uses the solar dish concentrator while the Eames system uses the solar collector. Also, the current cooling method is by use of TECMs condenser while the Eames system uses a heat exchanger between the feed water and the water vapor. Finally, the outputs of the present system are electricity and desalinated water, while Eames system provides only desalinated water. For the same major parameters, the results show a good agreement, as shown in Table 3. Eames system yields higher productivity due to the lower operating pressure and higher feed water temperature to the evaporator. However, the present proposed system produces electrical power, while the Eames

Table 4
Comparison of the proposed system at four different cases at solar radiation of 700 W/m^2, ambient temperature of 300 K, and wind speed of 5 m/s.

Case #	Components	$m_{disttilled}$ (kg/day)	P_{net} (W)	η_{system} (%)
Case 1	Stirling engine + Preheating + TEC modules + Vacuum evaporator	40.96	629	64.44
Case 2	Stirling engine + TEC + Vacuum evaporator	34.14	629	54.87
Case 3	Stirling engine + preheating + Vacuum evaporator	11.74	1126	34.53
Case 4	Stirling engine + Vacuum evaporator	2.39	1007	22.84

system consumed it.

4.2. Performance of the solar dish Stirling engine system

The performance of the solar dish Stirling engine system affected by number of uncontrollable parameters (such as the solar radiation and wind speed) and by controllable parameters selected by the designer (such as the solar dish diameter, reflectivity of the solar dish material, swept volume of the Stirling engine, working fluid of the Stirling engine, and the mass flow rate of the cooling water). The effects of these parameters on the performance of the system are discussed in this section.

Fig. 5(a and b, c, and d) shows the relationship between the solar radiation and the output power of the Stirling engine, Stirling engine efficiency, temperature of the HCSE(receiver), and the outlet temperature of the saline cooling water from the cold side of the Stirling engine, respectively. Also, Fig. 5 shows the effect of the wind speed on the same output parameters. It can be noted that the output power of the Stirling engine and its efficiency increases with the increase of the solar radiation (Fig. 5(a and b)). This indicates that the increase of the input energy is more than the increase in energy losses. However, at the same solar radiation, higher wind speed increases the losses to the ambient and decreases the output power and efficiency. These results correspond to those obtained by the theoretical model proposed by Lai et al. [51]. In summer season, at solar radiation of 700 W/m^2, wind speed of 5 m/s with a solar dish diameter of 2.68 m, the output power of the engine is 1200 W with an efficiency of 45.5%, hot chamber temperature of 820 K, and outlet temperature of the saline cooling water of 316 K. At solar radiation of 300 W/m^2, the engine output power is 550 W with an efficiency of 43%, hot chamber temperature of 580 K, and outlet temperature of the saline cooling water of 307 K.

Fig. 6(a and b) shows the relationship between the solar dish diameter with the output power of the SE and the outlet temperature of the saline cooling water for different working fluids of the SE. It is straightforward that a larger solar dish diameter provides higher output power due to the increase of the concentrated solar energy. Also, it can be noted that the generated power for hydrogen is two-to-three times higher than of the air (as shown in Fig. 6 (a)). This is returned to the thermodynamic properties of the hydrogen gas. It has the highest gas constant and low viscosity which increases the heat transfer coefficient of the absorbed heat by the engine and improves the efficiency of the Stirling engine. However, the use of hydrogen gas as a working fluid increases the risks due to its flammability. At solar dish diameter of 2.68 m, solar radiation intensity of 700 W/m^2, and wind speed of 5 m/s, the engine output power was 1400 W for air and 3200 W for hydrogen which is about two times higher than of the air. For the same conditions with a larger diameter of 4 m, the engine output power was 2400 W for the air and 7600 for the hydrogen which is about three times than of the air. That is mean the hydrogen gas is more preferred for large scale Stirling engine. Also, it can be noted that the engine output power with helium is close to that with hydrogen. So, for high output power and more safety, helium is more suitable than the other gases.

The rejected heat by the SE decreases as the output electrical power increases. The decrease of the rejected heat decreases the outlet temperature of the saline working fluid. Since the hydrogen gas provides the highest output electrical power, it also rejects the lowest amount of heat to the cooling water. So, the outlet temperature of the saline cooling water is minimum with the hydrogen gas as working fluid (see Fig. 6 (b)). Also, it is noted that the outlet temperature of the saline cooling water almost the same for the air and nitrogen that used as a working fluid. This is due to that the values of their gas constants are very close.

4.3. Performance of the TECMs system

The thermoelectric modules have a major function in the operation of the proposed system. So, the variation of their performance with the variation of the solar radiation intensity is discussed in this section. The outlet temperature of the saline water from the SE unit considered as the inlet temperature at the hot side of the TECMs. The absorbed heat by the saline water from the hot side of the TECMs further increases its temperature to the proper level of the vacuumed evaporation process. As mentioned before, higher solar radiation increases the outlet temperature of the saline water from the SE (see Fig. 7 (a)). This reduces the ability of the saline water to absorb the rejected heat from the hot side of the TECMs. So, higher temperatures resulted in the sides of the TECMs and the consumed power by the TECMs increases (see Fig. 7(b and c)). At a solar radiation of 700 W/m^2 and wind speed of 5 m/s, the outlet temperature of the saline water from the SE unit is 316 K and then heated by the TECMs to 327 K before entering the vacuum evaporator. At these conditions, the consumed power by the TECMs is 500 W, and the cold and hot side temperatures of the TECMs are 318 K and 328 K, respectively. The COP of the TECMs at the same conditions is 0.71.

4.4. Performance of the vacuum evaporator system

One of the main advantages of the system its ability to provides electricity and desalinated water. As mentioned before, the desalination process occurs by the evacuation of the evaporation chamber. In this section, the performance of the desalination unit with the variation of the solar radiation intensity is discussed. Fig. 8 (a) shows the estimated productivity of the desalinated water during the day (9 h) with the net output power of the system for different solar dish diameters. At a solar radiation of 700 W/m^2, wind speed of 5 m/s, and solar dish diameter of 2.68 m, a 15 kg/day with 1400 W net output power are obtained. At a solar dish diameter of 3.79 m, a 42 kg/day with 2000 W net output power is produced. Fig. 8 (b) shows the consumed power by the vacuum pump and the TECMs. As the saline water temperature increases, the required power to the evacuation process decreases while the needed power for condensation slightly increases. Finally, Fig. 8 (c) shows the overall efficiency of the system with the variation of the solar radiation for two solar dish diameters. Up to solar radiation of 800 W/m^2, the larger diameter dish system has a higher overall efficiency. For solar radiation more than 800 W/m^2, the consumed power by the vacuum pump and TECMs increases such that the overall efficiency starts to decline.

Table 4 shows a comparison between the performance of the proposed system at four cases. Case 1 presents the system with pre-heating process implemented by the recovery of the rejected heat from the cold side of the Stirling engine and with using TEC modules to enhance the condensation process inside the evaporator and to heat the saline water by the rejected heat from the hot side of the TEC modules. Case 2 is calculated using TEC modules only for heating process of the saline water and for condensation process inside the evaporator.

Case 3 is calculated without using TEC modules. In this case, the condensation process is performed by convection with ambient air and the saline water pre-heated only by the rejected heat from the Stirling engine. Case 4 is calculated without pre-heating process and without using TEC modules. As can be noted from Table 4, the pre-heating process (case 3) increases the productivity from 2.39 kg/day to 11.74 kg/day and the overall efficiency from 22.84% to 34.53%. This is because that the preheating process increases the temperature of the water which improves the evaporation and so the productivity of the distilled water. Also, the preheating process enhance the efficiency of the Stirling engine by the efficient cooling of the cold chamber. The TEC modules (without preheating, case 2) have greater effect in the productivity and the overall efficiency of the system. They increase the productivity from 2.39 kg/day to 34.24 kg/day and the efficiency from 22.84% to 54.87%. This is due to the efficient condensation by the cold side and the heating of the saline water by the hot side of the TEC modules. However, the net produced power is decreases from 1007 W to 629 W. Finally, the combination of the preheating process with TEC modules increases the productivity of the system from 2.93 kg/day to 40.96 kg/day and the overall efficiency of the system from 22.84% to 64.44%.

5. Conclusions

In this paper, a novel and interactive solar power generation and water desalination system has been introduced. The system composed of a solar dish Stirling engine unit used to generate electrical power, thermoelectric cooler modules (condenser), and vacuum evaporator. The saline water heated by the heat rejected from the Stirling engine and the TECMs. Part of the generated power used to operate the TECMs and the vacuum pump. A steady-state mathematical model has been introduced and validated by the comparison with similar theoretical and experimental published systems. The simulation process performed by the EES program and the results show that:

- The performance of the solar dish system is improved with high solar radiation intensity, low wind speed, large dish diameter, high solar dish reflectivity, low mass flow rate of the saline cooling water, and an optimized swept volume of the SE.
- The use of hydrogen gas as a working fluid of the SE provides the highest output power. However, the helium gas is more suitable for a high output power system with more safety than hydrogen.
- The performance of the TECMs is negatively affected by the increase of the solar radiation intensity.
- The performance of the vacuum evaporator is positively affected by the increase of the solar radiation intensity.
- The preheating process increase the productivity of the system from 2.93 kg/day to 11.74 kg/day. The TEC modules increase of the productivity from 2.39 kg/day to 34.14 kg/day. While the combination of the preheating and the TEC modules increases the productivity from 2.93 kg/day to 40.96 kg/day. However, the TEC modules consume about 45% of the output power of the Stirling engine.

Finally, at the specified parameters in Table 1 with a solar radiation of 700 W/m^2, wind speed of 5 m/s, and ambient temperature of 300 K, the output power of the SE is 1275 W, the consumed power by the TECMs is 506 W, the consumed power by the vacuum pump is 266.2 W, the net electrical output power is 502.8 W, and the daily desalinated water is 28 kg/day with an overall system efficiency of 65.8%, SE efficiency of 45%, a COP of the TECMs of 0.8, hot chamber temperature of 818 K, cold chamber temperature of 367K, and a saline water temperature at the inlet of the vacuum evaporator of 322 K.

Declaration of competing interest

The authors declare that they have no known competing financial interests or personal relationships that could have appeared to influence the work reported in this paper.

CRediT authorship contribution statement

Moh'd A. Al-Nimr: Conceptualization, Methodology, Validation, Writing - review & editing. **Wahib A. Al-Ammari:** Writing - original draft, Investigation, Software.

References

[1] O. Ogunmodimu, E.C. Okoroigwe, Concentrating solar power technologies for solar thermal grid electricity in Nigeria: a review, Renew. Sustain. Energy Rev. 90 (February) (2018) 104–119, https://doi.org/10.1016/j.rser.2018.03.029.
[2] L.S. Mendoza Castellanos, et al., Experimental analysis and numerical validation of the solar Dish/Stirling system connected to the electric grid, Renew. Energy 135 (2019) 259–265, https://doi.org/10.1016/j.renene.2018.11.095.
[3] J.P. Bijarniya, K. Sudhakar, P. Baredar, Concentrated solar power technology in India: a review, Renew. Sustain. Energy Rev. (2016), https://doi.org/10.1016/j.rser.2016.05.064.
[4] A.O. Onokwai, U.C. Okonkwo, C.O. Osueke, C.E. Okafor, T.M.A. Olayanju, S.O. Dahunsi, Design, modelling, energy and exergy analysis of a parabolic cooker, Renew. Energy 142 (2019) 497–510, https://doi.org/10.1016/j.renene.2019.04.028.
[5] T. Arunkumar, et al., A review of efficient high productivity solar stills, Renew. Sustain. Energy Rev. 101 (November) (2019) 197–220, https://doi.org/10.1016/j.rser.2018.11.013.
[6] R. Karimi, T.T. Gheinani, V. Madadi Avargani, Coupling of a parabolic solar dish collector to finned-tube heat exchangers for hot air production: an experimental and theoretical study, Sol. Energy 187 (May) (2019) 199–211, https://doi.org/10.1016/j.solener.2019.05.050.
[7] E.I. Eid, R.A. Khalaf-Allah, A.M. Soliman, A.S. Easa, Performance of a beta Stirling refrigerator with tubular evaporator and condenser having inserted twisted tapes and driven by a solar energy heat engine, Renew. Energy 135 (2019) 1314–1326, https://doi.org/10.1016/j.renene.2018.09.044.
[8] B. Ghorbani, R. Shirmohammadi, M. Mehrpooya, Development of an innovative cogeneration system for fresh water and power production by renewable energy using thermal energy storage system, Sustain. Energy Technol. Assess. 37 (November 2019) (2020) 100572, https://doi.org/10.1016/j.seta.2019.100572.
[9] F. Jabari, M. Nazari-heris, B. Mohammadi-ivatloo, S. Asadi, A solar dish Stirling engine combined humidification-dehumidification desalination cycle for cleaner production of cool , pure water , and power in hot and humid regions, Sustain. Energy Technol. Assess. 37 (August 2019) (2020) 100642, https://doi.org/10.1016/j.seta.2020.100642.
[10] R. Loni, A.B. Kasaeian, O. Mahian, A.Z. Sahin, Thermodynamic analysis of an organic rankine cycle using a tubular solar cavity receiver, Energy Convers. Manag. (2016), https://doi.org/10.1016/j.enconman.2016.09.007.
[11] P.D. Malali, S.K. Chaturvedi, T. Abdel-Salam, Performance optimization of a regenerative Brayton heat engine coupled with a parabolic dish solar collector, Energy Convers. Manag. 143 (2017) 85–95, https://doi.org/10.1016/j.enconman.2017.03.067.
[12] M.S. Khan, M. Abid, H.M. Ali, K.P. Amber, M.A. Bashir, S. Javed, Comparative performance assessment of solar dish assisted s-CO2 Brayton cycle using nanofluids, Appl. Therm. Eng. 148 (July 2018) (2019) 295–306, https://doi.org/10.1016/j.applthermaleng.2018.11.021.
[13] S.Y. Wu, L. Xiao, Y. Cao, Y.R. Li, A parabolic dish/AMTEC solar thermal power system and its performance evaluation, Appl. Energy 87 (2) (2010) 452–462, https://doi.org/10.1016/j.apenergy.2009.08.041.
[14] Y.M. Seshie, K.E. N'Tsoukpoe, P. Neveu, Y. Coulibaly, Y.K. Azoumah, Small scale concentrating solar plants for rural electrification, Renew. Sustain. Energy Rev. 90 (February) (2018) 195–209, https://doi.org/10.1016/j.rser.2018.03.036.
[15] J. Coventry, C. Andraka, Dish systems for CSP, Sol. Energy (2017), https://doi.org/10.1016/j.solener.2017.02.056.

[16] L.S. Mendoza Castellanos, et al., Experimental analysis and numerical validation of the solar Dish/Stirling system connected to the electric grid, Renew. Energy (June) (2019) 259–265, https://doi.org/10.1016/j.renene.2018.11.095.
[17] S. Mendoza, et al., Mathematical modeling of the geometrical sizing and thermal performance of a Dish/Stirling system for power generation Mathematical modeling of the geometrical sizing and thermal performance of a Dish/Stirling system for power generation, Renew. Energy 107 (January 2017) (2019) 23–35, https://doi.org/10.1016/j.renene.2017.01.020.
[18] A.Z. Hafez, A. Soliman, K.A. El-Metwally, I.M. Ismail, Solar parabolic dish Stirling engine system design, simulation, and thermal analysis, Energy Convers. Manag. 126 (2016) 60–75, https://doi.org/10.1016/j.enconman.2016.07.067.
[19] A.M.A. Al-Dafaie, M.E. Dahdolan, M.A. Al-Nimr, Utilizing the heat rejected from a solar dish Stirling engine in potable water production, Sol. Energy 136 (2016) 317–326, https://doi.org/10.1016/j.solener.2016.07.007.
[20] G.O. Prado, L.G.M. Vieira, J.J.R. Damasceno, Solar dish concentrator for desalting water, Sol. Energy 136 (2016) 659–667, https://doi.org/10.1016/j.solener.2016.07.039.
[21] M. Bahrami, V. Madadi Avargani, M. Bonyadi, Comprehensive experimental and theoretical study of a novel still coupled to a solar dish concentrator, Appl. Therm. Eng. (2019) 77–89, https://doi.org/10.1016/j.applthermaleng.2019.01.103.
[22] K. Karthick, S. Suresh, M.M.M.D. Hussain, H.M. Ali, C.S.S. Kumar, Evaluation of solar thermal system configurations for thermoelectric generator applications: a critical review, Sol. Energy 188 (March) (2019) 111–142, https://doi.org/10.1016/j.solener.2019.05.075.
[23] D. Champier, Thermoelectric generators: a review of applications, Energy Convers. Manag. 140 (2017) 167–181, https://doi.org/10.1016/j.enconman.2017.02.070.
[24] D. Zhao, G. Tan, A review of thermoelectric cooling: materials, modeling and applications, Appl. Therm. Eng. 66 (1–2) (2014) 15–24, https://doi.org/10.1016/j.applthermaleng.2014.01.074.
[25] S. Dubey, J.N. Sarvaiya, B. Seshadri, Temperature dependent photovoltaic (PV) efficiency and its effect on PV production in the world – a review, Energy Procedia 33 (Jan. 2013) 311–321, https://doi.org/10.1016/J.EGYPRO.2013.05.072.
[26] N. Dimri, A. Tiwari, G.N. Tiwari, Effect of thermoelectric cooler (TEC) integrated at the base of opaque photovoltaic (PV) module to enhance an overall electrical efficiency, Sol. Energy 166 (November 2017) (2018) 159–170, https://doi.org/10.1016/j.solener.2018.03.030.
[27] A.A. Dehghan, A. Afshari, N. Rahbar, Thermal modeling and exergetic analysis of a thermoelectric assisted solar still, Sol. Energy 115 (2015) 277–288, https://doi.org/10.1016/j.solener.2015.02.038.
[28] N. Rahbar, J.A. Esfahani, A. Asadi, An experimental investigation on productivity and performance of a new improved design portable asymmetrical solar still utilizing thermoelectric modules, Energy Convers. Manag. 118 (2016) 55–62, https://doi.org/10.1016/j.enconman.2016.03.052.
[29] M.A. Al-Nimr, W.A. Al-Ammari, A. Alkhalidi, A novel hybrid photovoltaics/thermoelectric cooler distillation system, Int. J. Energy Res. 43 (2) (2019) 791–805, https://doi.org/10.1002/er.4309.
[30] H. Al-Madhhachi, G. Min, Effective use of thermal energy at both hot and cold side of thermoelectric module for developing efficient thermoelectric water distillation system, Energy Convers. Manag. 133 (2017) 14–19, https://doi.org/10.1016/j.enconman.2016.11.055.
[31] M. Jradi, N. Ghaddar, K. Ghali, Experimental and theoretical study of an integrated thermoelectric-photovoltaic system for air dehumidification and fresh water production, Int. J. Energy Res. (2012), https://doi.org/10.1002/er.1848.
[32] P. Byrne, et al., A review on the coupling of cooling, desalination and solar photovoltaic systems, Renew. Sustain. Energy Rev. 47 (2015) 703–717, https://doi.org/10.1016/j.rser.2015.03.083.
[33] A. Subramani, M. Badruzzaman, J. Oppenheimer, J.G. Jacangelo, Energy minimization strategies and renewable energy utilization for desalination: a review, Water Res. 45 (5) (Feb. 2011) 1907–1920, https://doi.org/10.1016/J.WATRES.2010.12.032.
[34] H. Sharon, K.S. Reddy, A review of solar energy driven desalination technologies, Renew. Sustain. Energy Rev. 41 (2015) 1080–1118, https://doi.org/10.1016/j.rser.2014.09.002.
[35] A. Rashid, T. Ayhan, A. Abbas, Natural vacuum distillation for seawater desalination – a review, Desalin. Water Treat. 57 (56) (2016) 26943–26953, https://doi.org/10.1080/19443994.2016.1172264.
[36] V. Sriram, Kanimozhi, A. Anderson, Desalination at low temperature and low pressure, Int. J. Appl. Eng. Res. 9 (24) (2014) 24415–24424, https://doi.org/10.1016/j.desal.2008.06.005.
[37] K.S. Reddy, K.R. Kumar, T.S. O'Donovan, T.K. Mallick, Performance analysis of an evacuated multi-stage solar water desalination system, Desalination 288 (2012) 80–92, https://doi.org/10.1016/j.desal.2011.12.016.
[38] M.J. Abbaspour, M. Faegh, M.B. Shafii, Experimental examination of a natural vacuum desalination system integrated with evacuated tube collectors, Desalination 467 (June) (2019) 79–85, https://doi.org/10.1016/j.desal.2019.06.004.
[39] N.S. Myneni, A. Date, M. Ward, P. Gokhale, M. Gay, Combined thermoelectric power generation and passive vacuum desalination, Energy Procedia 110 (December 2016) (2017) 262–267, https://doi.org/10.1016/j.egypro.2017.03.137.
[40] H. Ambarita, Study on the performance of natural vacuum desalination system using low grade heat source, Case Stud. Therm. Eng. 8 (August) (2016) 346–358, https://doi.org/10.1016/j.csite.2016.09.005.
[41] G. Venkatesan, S. Iniyan, P. Jalihal, A desalination method utilising low-grade waste heat energy, Desalin. Water Treat. 56 (8) (2015) 2037–2045, https://doi.org/10.1080/19443994.2014.960459.
[42] F. Incropera, D. Dewitt, T. Bergman, A. Lavine, Introduction, in: Principles of Heat and Mass Transfer, 2013, pp. 1–49.
[43] Y.H. Zurigat, M.K. Abu-Arabi, Modelling and performance analysis of a regenerative solar desalination unit, Appl. Therm. Eng. 24 (7) (2004) 1061–1072, https://doi.org/10.1016/j.applthermaleng.2003.11.010.
[44] N. Akhtar, S.C. Mullick, Computation of glass-cover temperatures and top heat loss coefficient of flat-plate solar collectors with double glazing, Energy 32 (7) (2007) 1067–1074, https://doi.org/10.1016/j.energy.2006.07.007.
[45] J.H. Shazly, A.Z. Hafez, E.T. El Shenawy, M.B. Eteiba, Simulation, design and thermal analysis of a solar Stirling engine using MATLAB, Energy Convers. Manag. 79 (2014) 626–639, https://doi.org/10.1016/j.enconman.2014.01.001.
[46] F. Incropera, D. Dewitt, T. Bergman, A. Lavine, Free convection, in: Principles of Heat and Mass Transfer, 2013, pp. 593–631.
[47] Y. Cengel, Heat transfer: a practical approach, J. Chem. Inf. Model. (2013), https://doi.org/10.1017/CBO9781107415324.004.
[48] H. Lee, Appendix B: thermoelectrics, in: Thermal Design, 2010.
[49] G.A. Bemporad, Basic hydrodynamic aspects of a solar energy 54 (2) (1995) 125–134.
[50] I.W. Eames, G.G. Maidment, A.K. Lalzad, A theoretical and experimental investigation of a small-scale solar-powered barometric desalination system, Appl. Therm. Eng. 27 (11–12) (2007) 1951–1959, https://doi.org/10.1016/j.applthermaleng.2006.12.015.
[51] X. Lai, M. Yu, R. Long, Z. Liu, W. Liu, Dynamic performance analysis and optimization of dish solar Stirling engine based on a modified theoretical model, Energy 183 (2019) 573–583, https://doi.org/10.1016/j.energy.2019.06.131.